

## Saturation of the Rayleigh-Taylor Growth of Broad-Bandwidth Laser-Imposed Nonuniformities in Planar Targets

V. A. Smalyuk,<sup>1,\*</sup> T. R. Boehly,<sup>1</sup> D. K. Bradley,<sup>1</sup> V. N. Goncharov,<sup>1</sup> J. A. Delettrez,<sup>1</sup> J. P. Knauer,<sup>1</sup>  
D. D. Meyerhofer,<sup>1,\*†</sup> D. Oron,<sup>2</sup> and D. Shvarts<sup>2</sup>

<sup>1</sup>Laboratory for Laser Energetics, University of Rochester, 250 East River Road, Rochester, New York 14623

<sup>2</sup>Department of Physics, Nuclear Research Center Negev, Beer-Sheva, Israel

(Received 4 September 1998)

The Rayleigh-Taylor evolution of 3D broadband perturbations seeded by 351-nm laser nonuniformities was measured in accelerated planar targets using x-ray radiography at  $\sim 1.3$  keV. Fourier analysis shows that the perturbations evolve to longer wavelengths with shorter wavelengths saturating. The saturation amplitudes and rates of growth of 3D features are consistent with the predictions of Haan [Phys. Rev. A **39**, 5812 (1989)]. [S0031-9007(98)07891-0]

PACS numbers: 52.35.Py, 52.50.Jm, 52.70.La

In inertial confinement fusion (ICF), the Rayleigh-Taylor (RT) instability can amplify target perturbations sufficiently to disrupt the implosion and degrade its performance [1]. These perturbations can result from existing target imperfections or, in the case of direct-drive ICF, also from laser imprinting [2]. To achieve high-gain ICF, one must control laser imprinting and the hydrodynamic stability of the targets [3]. In addressing the latter, target designs rely on the predicted saturation of unstable growth by nonlinear effects. It is therefore critical to the success of ICF that this saturation be measured and understood. In recent years, several models have been developed to explain nonlinear broadband RT evolution in Fourier [4–9] and real [9–11] space. Some multimode nonlinear behavior has been measured in indirect-drive RT experiments with preimposed 3D multimode initial perturbations in planar targets [12,13]. Signatures of nonlinear behavior have been measured in several works [2,14–16] using laser imprint as the initial perturbation for RT growth, but only qualitative analysis of broadband saturation effects was shown. We present the results of experiments where 3D broadband imprinted features exhibit growth that saturates at amplitudes consistent with the model of Haan [4]. We believe this is the first clear demonstration of such behavior in conditions relevant to ICF.

In our experiment, initially smooth, 20- $\mu\text{m}$ -thick CH targets ( $\rho = 1.05$  g/cm<sup>3</sup>) were irradiated at  $2 \times 10^{14}$  W/cm<sup>2</sup> in 3-ns square pulses by five overlapping UV beams. To enhance the on-target uniformity, all five beams had distributed phase plates (DPP's) [17], smoothing by spectral dispersion (SSD) [18], and distributed polarization rotators (DPR's) [2]. The targets were backlit with x rays produced by a uranium backlighter irradiated at  $\sim 1 \times 10^{14}$  W/cm<sup>2</sup> (using twelve additional beams). X rays transmitted through the target and a 3- $\mu\text{m}$ -thick aluminum blast shield were imaged by 8- $\mu\text{m}$  pinholes on a framing camera filtered with 6  $\mu\text{m}$  of aluminum. This yielded the highest sensitivity for an average photon energy of  $\sim 1.3$  keV. The framing

camera produced eight temporally displaced images of  $\sim 80$ -ps duration and magnification of 14. The measured target optical depth (OD) is obtained from the natural logarithm of the intensity-converted images captured on Kodak T-Max 3200 film.

The primary experiment involved six shots, performed with identical drive conditions and radiographs obtained at different times. For each shot, up to six images of the same area of the target were processed with a 400- $\mu\text{m}$  analysis box. These images were acquired during the time interval from 1.5 to 2.8 ns after the beginning of the drive. The backlighter shape was removed by subtracting a fourth-order, two-dimensional envelope fit to data. The resulting images are the measured modulations of optical depth  $D_m(\mathbf{f})$ . Using the measured system resolution, noise, and sensitivity, we applied a Wiener filter to remove the noise from the images and deconvolved the system's modulation transfer function to recover the target's areal density modulations  $D_t(\mathbf{f})$  [19]. The noise in these measurements is determined by the photon statistics of the backlighter x rays, and the system resolution is limited by the 8- $\mu\text{m}$  pinhole. Three fully processed images of the target optical depth at 1.9, 2.3, and 2.4 ns are shown in Fig. 1 for one of the six shots. It has been found that nonuniform shocks can produce areal density modulations (in the bulk of a target) which are comparable to those

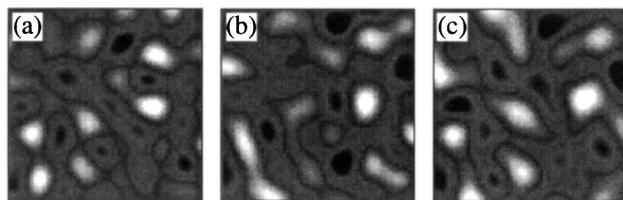


FIG. 1. Fully processed subimages (with a box size of 100  $\mu\text{m}$ ) of the target optical depth captured at (a) 1.9, (b) 2.3, and (c) 2.4 ns for one of the six shots taken with laser conditions that include DPP's, SSD, and DPR's. The evolution in time to longer-scale structures is evident.

from the amplitude modulation at the ablation surface [20]. However, after about  $\sim 1$  ns of drive, modulations with spatial frequencies in the region of  $10\text{--}100\text{ mm}^{-1}$  (where these measurements are performed) experience sufficient RT growth to dominate any density modulation produced by nonuniform shocks. The measured modulations therefore represent the amplitude at the ablation surface well.

In the linear regime of the RT instability, each individual mode grows exponentially at a rate  $\gamma$ , determined by the dispersion relation [21]

$$\gamma = \alpha \sqrt{\frac{kg}{1 + kL_m}} - \beta kV_a, \quad (1)$$

where  $k$  is the mode wave number,  $g$  is a target acceleration,  $L_m$  is the density-gradient scale length, and  $V_a$  is the ablation velocity. For CH targets and drive intensities  $\sim 10^{14}\text{ W/cm}^2$ ,  $L_m \approx 1\text{ }\mu\text{m}$  and the constants  $\alpha \approx 1$  and  $\beta \approx 1.7$  determine how the actual growth rate differs from the classical one. For a single-mode initial perturbation, nonlinear effects create bubbles and spikes [5,8,9] and cause the exponential growth of the mode to saturate at an amplitude  $Z_k \approx 0.1\lambda$  and to subsequently grow at constant velocity [4].

The evolution of 3D broadband perturbations is more complicated. The fastest-growing modes rapidly drive harmonics and coupled modes. The contribution due to mode coupling becomes comparable to the exponential growth for some of the modes even at small (in the linear regime) amplitudes. As a result, some modes grow faster than others, while others shrink and change their phases [8]; however, the average amplitude of all modes at given spatial frequency grows exponentially at the rate given in Eq. (1). Saturation occurs due to collective behavior of the modes because adjacent modes can constructively interfere to create local structures with amplitudes much larger than those of individual modes. As these features experience saturation, the individual modes saturate at amplitudes much less than  $0.1\lambda$ . After reaching saturation level, the modes grow, on average, at constant velocity with a continuous transition from linear to nonlinear stages. Haan formulated a model for the saturation of 3D broadband spectrum and found a saturation level of the azimuthally averaged amplitude given by [6,7]

$$S(k) = 2/Lk^2, \quad (2)$$

where  $L$  is the size of the analysis box. The  $L$  dependence occurs because the individual Fourier amplitudes of the broadband features depend on the size of the analysis region (i.e., the number of Fourier modes decreases as the box size is reduced, whereas the rms amplitude does not).

The behavior predicted by this model is shown in Fig. 2(a) for an initial perturbation spectrum that has constant power per mode as a function of spatial frequency. This is representative of the features imprinted by irradiation nonuniformities that arise primarily from the speckle

pattern produced by DPP's and SSD [22]. The evolution of this spectrum (plotted as the average amplitudes versus spatial frequency for seven different times between  $t = 1.3$  to  $2.2$  ns) is simply modeled by applying the growth-rate dispersion relation [Eq. (1)] and the saturation level [Eq. (2)], where the target acceleration was  $g = 50\text{ }\mu\text{m/ns}^2$ , ablation velocity  $V_a = 2.5\text{ }\mu\text{m/ns}$ , and the nonuniformity's  $\sigma_{\text{rms}} = 0.03\text{ }\mu\text{m}$ . The amplitudes are converted to target optical depth by dividing by the measured, spectrally weighed, attenuation length  $\lambda_x = 10 \pm 2\text{ }\mu\text{m}$  and multiplying by the simulated compression of the target (about 2 for times from 1.6 to 2.6 ns). The high-frequency modes grow most rapidly and saturate at the level given by Eq. (2), while the low-frequency modes grow more slowly. As a result, the midfrequency modes experience the largest growth factors, producing a peak in the spectrum. As the evolution progresses, the midfrequency modes begin to saturate, and that peak moves to longer wavelengths. This behavior is relatively insensitive to the initial spectrum or drive conditions, therefore, most broad-bandwidth initial spectra will evolve similarly given sufficient time. Variations in growth rates of up to 50%, or the  $\sigma_{\text{rms}}$  of initial spectrum up to 2 orders of magnitude, have little effect on the predicted spectral evolution; the only condition is that the spectrum be broadband. We have demonstrated this by experimentally varying the initial imprint spectrum using different levels of laser-beam smoothing. The result is that the late-time evolution of target nonuniformities is insensitive to the initial conditions, or the drive characteristics. It is therefore reasonable to use the simple model shown (as opposed to complex simulations) to predict the effect of saturation in spectral evolution.

The evolution of averaged amplitudes of measured target optical depth as the function of spatial frequency for two shots with planar  $20\text{-}\mu\text{m}$  CH targets is shown in Fig. 2(b) for times of 1.4 to 2.2 ns and in Fig. 2(c) for somewhat later times of 1.6 to 2.4 ns. To obtain the average amplitudes, the Fourier amplitudes are azimuthally averaged at each spatial frequency. One can readily see that the measured spectra are peaked and that the peak shifts toward longer wavelengths as time progresses, similar to the predicted behavior shown in Fig. 2(a). Moreover, the dashed line which shows the Haan saturation level is in reasonable agreement. Similar behavior was observed for all six shots taken under identical drive conditions.

From Figs. 2(b) and 2(c), one can see that the measured growth of the amplitudes at  $20\text{-}\mu\text{m}$  wavelength is much less pronounced than that of  $30$  and  $60\text{ }\mu\text{m}$  for the time interval of 1.5 to 2.5 ns. This is because the amplitudes at  $20\text{ }\mu\text{m}$  are predicted to be already above Haan's saturation level, while amplitudes at  $30\text{ }\mu\text{m}$  experience a transition from exponential growth to the saturated growth with constant velocity. The amplitude at  $60\text{ }\mu\text{m}$  is predicted not to be saturated and therefore should grow exponentially during this time interval. To support the above

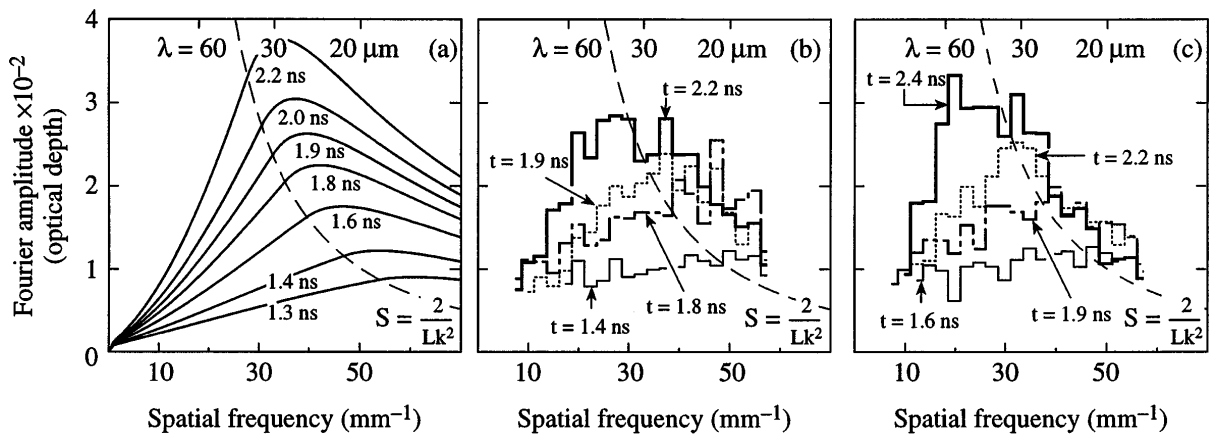


FIG. 2. (a) Predicted Fourier amplitudes of optical depth using the Haan model for an assumed spectrum of perturbations with initial flat power per mode ( $\sigma_{rms} = 0.03 \mu\text{m}$ ) spectrum and  $L = 400 \mu\text{m}$  at times 1.3, 1.4, 1.6, 1.8, 1.9, 2.0, and 2.2 ns. (b) The measured azimuthally averaged Fourier amplitudes of the optical depth modulations as a function of spatial frequency for 20- $\mu\text{m}$ -thick foil at times 1.4, 1.8, 1.9, and 2.2 ns. (c) The same for another shot with 20- $\mu\text{m}$ -thick foil at times 1.6, 1.9, 2.2, and 2.4 ns. Haan's saturation amplitude  $S$  is shown by the dashed line.

observations, we measured the growth of preimposed, 2D, 60- $\mu\text{m}$ -wavelength and 30- $\mu\text{m}$ -wavelength single-mode, sinusoidal perturbations on 20- $\mu\text{m}$ -thick CH foils, driven with the same irradiation conditions. Targets with initial perturbation amplitudes of 0.05 and 0.125  $\mu\text{m}$  at 60- $\mu\text{m}$  wavelength and 0.025  $\mu\text{m}$  at 30- $\mu\text{m}$  wavelength were used. These initial amplitudes are sufficiently low that even after 2.5 ns of the drive they are expected to be in the linear regime, yet have high enough amplitudes that mode coupling from the broadband spectrum has no effect on their evolution. Figure 3(a) shows that the broadband features at 60  $\mu\text{m}$  (the combined data from six shots) grow at a similar rate as the preimposed 60- $\mu\text{m}$  modulations (upper data points for two shots). Exponential fits to these data (three solid lines) indicate growth rates of  $0.96 \pm 0.02 \text{ ns}^{-1}$  and  $1.02 \pm 0.02 \text{ ns}^{-1}$  for the preimposed modulations and  $0.91 \pm 0.05 \text{ ns}^{-1}$  for the broadband modulations. Figure 3(b) shows that the broadband features at 30  $\mu\text{m}$  (the combined data from six shots) experience a transition from linear to nonlinear phases at an amplitude of about 0.02 OD, which is 30 times lower than the single-mode saturation value of 0.6 OD ( $0.1\lambda$ ). At the same time, the two preimposed 30- $\mu\text{m}$  modulations (upper data points) grow exponentially with growth rates of  $1.45 \pm 0.02 \text{ ns}^{-1}$  and  $1.54 \pm 0.02 \text{ ns}^{-1}$ , respectively. These measured growth rates for 60- $\mu\text{m}$  and 30- $\mu\text{m}$  preimposed modulations are smaller by a factor of 2.5 than those measured for earlier times (from 0 to 1.2 ns) by Knauer [20] in similar experiments but for larger amplitudes of initial preimposed modulations ( $a_0 = 0.5 \mu\text{m}$ ). This effect can be attributed to the finite foil thickness since the estimated late-time  $\sigma_{rms}$  amplitude ( $\sim 3 \mu\text{m}$ ), based on the measured spectra, is comparable to the thickness of a target ( $\sim 6 \mu\text{m}$ ) and may reduce the growth of these perturbations. If small-scale bubbles penetrate the target, the mass available to feed the growth

of a spike is limited, thereby limiting the perturbation growth [23].

To confirm that the saturation level and the late-time spectra depend on neither the target thickness nor the initial spectra of nonuniformity, we show in Fig. 4 the results of two additional experiments using a laser drive with DPP's only for 20- and 40- $\mu\text{m}$  foil thicknesses. Figure 4(a) shows the measured spectra at 1.0, 1.6, and 1.8 ns for one of the three shots performed with DPP's only on a 20- $\mu\text{m}$ -thick foil. The saturation level was calculated using the simulated compression of the target (about 2.5 for times from 1.0 to 1.8 ns). Figure 4(b) shows the measured spectra for 40- $\mu\text{m}$  CH foil at 2.7 and 2.8 ns for one of two shots. The saturation level was again calculated using the spectrally weighed attenuation

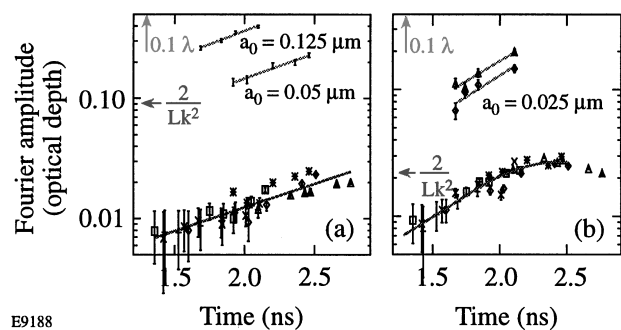


FIG. 3. (a) Average Fourier amplitudes of optical depth of imprinted features versus time at 60- $\mu\text{m}$  wavelength for six shots (distinguished by different symbols) and the amplitude of preimposed 60- $\mu\text{m}$  perturbations of corrugated targets with initial amplitudes of 0.05 and 0.125  $\mu\text{m}$  (upper data). (b) The same for the 30- $\mu\text{m}$  wavelength with the amplitudes of initial preimposed 30- $\mu\text{m}$  perturbations of 0.025  $\mu\text{m}$  (upper data). Exponential fits (solid lines) were used for the preimposed corrugation data and the 60- $\mu\text{m}$  imprinted data, and a third-order polynomial fit was used to the imprinted data at 30- $\mu\text{m}$ .

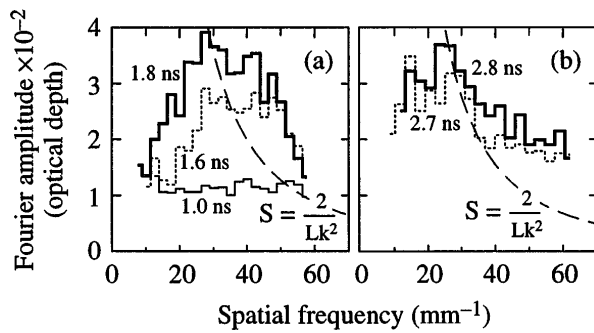


FIG. 4. Experimentally measured perturbation spectra using DPP-only drive beams. Azimuthally averaged Fourier amplitude of the optical depth modulation as a function of spatial frequency for (a) one of the three shots with 20- $\mu\text{m}$ -thick foil at 1.0, 1.6, and 1.8 ns and (b) one of the two shots with 40- $\mu\text{m}$ -thick foil at 2.7 and 2.8 ns. The saturation amplitude  $S$  is shown by the dashed line.

length  $\lambda_x$  (which does not change significantly going from 20- to 40- $\mu\text{m}$  foils) and the predicted compression (about 2 at 2–3 ns). It can be seen that (i) the higher amplitudes at early times [compare Fig. 4(a) to Figs. 2(b) and 2(c)] demonstrate that without SSD and DPR's the laser imprint is higher (ii) the finite target thickness does not affect the saturation levels since the shapes of measured spectra are similar for both thicknesses and in agreement with Haan's model, and (iii) the measured spectra for DPP-only laser drive (Fig. 4) have slightly higher amplitudes at spatial frequencies  $>40 \text{ mm}^{-1}$  than for the laser drive with all smoothing [Fig. 2(b) and 2(c)], indicating that SSD affects the shape of the initial imprint spectrum by lowering the amplitudes of high spatial frequencies [22].

This Letter has presented the measured evolution of 3D broadband perturbations produced by laser imprinting in CH foils, accelerated by UV light. Using through-foil radiography, the growth of these features was observed to saturate at levels in agreement with those predicted by Haan [4] and are much lower than the single-mode saturation levels  $0.1\lambda$ . This behavior was noted in both the shape of the spatial Fourier spectra and in the temporal behavior of modes at various wavelengths. In addition, we noted that the growth of perturbations from

a broadband spectrum in the linear regime is the same as that for the linear growth of preimposed 2D perturbations, also in agreement with the Haan model.

This work was supported by the U.S. Department of Energy Office of Inertial Confinement Fusion under Cooperative Agreement No. DE-FC03-92SF19460, the University of Rochester, and the New York State Energy Research and Development Authority. The support of DOE does not constitute an endorsement by DOE of the views expressed in this article.

\*Also at Department of Mechanical Engineering.

†Also at Department of Physics and Astronomy.

- [1] D. K. Bradley *et al.*, *Phys. Plasmas* **5**, 1870 (1998).
- [2] T. R. Boehly *et al.*, in *Laser Interaction and Related Plasma Phenomena*, edited by G. H. Miley and E. M. Campbell, AIP Conf. Proc. No. 406 (AIP, New York, 1997), p. 122.
- [3] S. E. Bodner *et al.*, *Phys. Plasmas* **5**, 1901 (1998).
- [4] S. W. Haan, *Phys. Rev. A* **39**, 5812 (1989).
- [5] S. W. Haan, *Phys. Fluids B* **3**, 2349 (1991).
- [6] M. J. Dunning *et al.*, *Phys. Plasmas* **2**, 1669 (1995).
- [7] J. P. Dahlburg *et al.*, *Phys. Plasmas* **2**, 2453 (1995).
- [8] D. Ofer *et al.*, *Phys. Plasmas* **3**, 3073 (1996).
- [9] D. Shvarts *et al.*, *Phys. Plasmas* **2**, 2465 (1995).
- [10] U. Alon *et al.*, *Phys. Rev. Lett.* **74**, 534 (1995).
- [11] D. Oron *et al.*, *Phys. Plasmas* **5**, 1467 (1998).
- [12] M. M. Marinak *et al.*, *Phys. Rev. Lett.* **75**, 3677 (1995).
- [13] M. M. Marinak *et al.*, *Phys. Rev. Lett.* **80**, 4426 (1998).
- [14] B. A. Remington *et al.*, *Phys. Fluids B* **5**, 2589 (1993).
- [15] R. J. Taylor *et al.*, *Phys. Rev. Lett.* **76**, 1643 (1996).
- [16] C. J. Pawley *et al.*, *Phys. Plasmas* **4**, 1969 (1997).
- [17] Y. Lin, T. J. Kessler, and G. N. Lawrence, *Opt. Lett.* **20**, 764 (1995).
- [18] S. Skupsky *et al.*, *J. Appl. Phys.* **66**, 3456 (1989).
- [19] V. A. Smalyuk *et al.*, *Rev. Sci. Instrum.* (to be published).
- [20] J. P. Knauer *et al.*, in *Laser Interaction and Related Plasma Phenomena*, edited by G. H. Miley and E. M. Campbell, AIP Conf. Proc. 406 (AIP, Woodbury, NY, 1997).
- [21] R. Betti *et al.*, *Phys. Plasmas* **5**, 1446 (1998).
- [22] S. Skupsky (private communication).
- [23] D. Oron *et al.*, "Proceedings of the 28th Annual Anomalous Absorption Conference, Bar Harbor, ME, 1998."